Biosensors and Bioelectronics 168 (2020) 112523

Contents lists available at ScienceDirect

Biosensors and Bioelectronics

journal homepage: http://www.elsevier.com/locate/bios

A designed whole-cell biosensor for live diagnosis of gut inflammation through nitrate sensing

Seung-Gyun Woo [a,b], Sung-Je Moon [b,c], Seong Keun Kim [a], Tae Hyun Kim [a,b], Hyun Seung Lim [a], Gun-Hwi Yeon [a,b], Bong Hyun Sung [a,b], Chul-Ho Lee [b,c], Seung-Goo Lee [a,b,**], Jung Hwan Hwang [b,c,***], Dae-Hee Lee [a,b,*]

[a] Synthetic Biology and Bioengineering Research Center, Korea Research Institute of Bioscience and Biotechnology (KRIBB), Daejeon, 34141, Republic of Korea
[b] Department of Biosystems and Bioengineering, KRIBB School of Biotechnology, University of Science and Technology (UST), Daejeon, 34113, Republic of Korea
[c] Laboratory Animal Resource Center, Korea Research Institute of Bioscience and Biotechnology (KRIBB), Daejeon, 34141, Republic of Korea

ARTICLE INFO

Keywords:
Whole cell biosensor
Gut inflammation
Designer probiotic
Nitrate sensing
Thiosulfate sensing
Boolean AND gate

ABSTRACT

Microbes reprogrammed using advanced genetic circuits are envisaged as emerging living diagnostics for a wide range of diseases and play key roles in regulating gut microbiota to treat disease-associated symptoms in a non-invasive manner. Here, we developed a designer probiotic *Escherichia coli* that senses and responds to nitrate, a biomarker of gut inflammation. To this end, we first employed the NarX-NarL two-component regulatory system in *E. coli* to construct a nitrate-responsive genetic circuit. Next, we optimized the nitrate biosensor for the best performance using measures of sensitivity and specificity. We then introduced this genetic circuit into a probiotic *E. coli* Nissle 1917. We demonstrated that the designed biosensor can sense elevated nitrate levels during gut inflammation in mice with native gut microbiota. Moreover, using Boolean AND gate, we generated a genetically encoded biosensor for simultaneous sensing of the thiosulfate and nitrate biomarkers, thus increasing the tool's specificity for diagnosing gut inflammation. The nitrate-responsive genetic circuit will enable new approaches for non-invasive diagnostics of inflammation-associated diseases.

1. Introduction

Synthetic biology has provided various genetic circuits that allow microorganisms to sense input signals and respond to them via reprogramming cellular functions (Xie and Fussenegger, 2018). Recent advances in the design-build-test-learn cycle of genetic circuits have enabled the application of engineered bacteria for living diagnostics and therapeutics (Riglar and Silver, 2018). In particular, probiotics have been actively serving as a chassis and have been reprogrammed through genetic circuits to sense disease biomarkers and to deliver therapeutics efficiently with site specificity (Singh et al., 2017). Similar to commensal bacteria in the gut, these designer probiotics can also sense, respond to, and control the gut environment (Hwang and Chang, 2020; Pham et al., 2017).

The mammalian gut is home to a diverse community of commensal, symbiotic, and even pathogenic microbes (Mimee et al., 2016) and plays active roles in human health, including metabolism (Fischbach and Sonnenburg, 2011), immunity (Belkaid and Hand, 2014), and the gut-brain axis (Sampson and Mazmanian, 2015). These interactions between the human host and microbes make the microbiota an attractive avenue for designer probiotics that can expand their functional repertoire through genetic circuits. Because the gut environment is mostly inaccessible, programmed probiotics can be employed as non-invasive diagnostics to sense molecules of interest in the gut or as therapeutics (Riglar et al., 2017). In this context, probiotic or commensal bacteria have been engineered to sense the biomarkers of

* Corresponding author. Synthetic Biology and Bioengineering Research Center, Korea Research Institute of Bioscience and Biotechnology (KRIBB), Daejeon, 34141, Republic of Korea.
** Corresponding author. Synthetic Biology and Bioengineering Research Center, Korea Research Institute of Bioscience and Biotechnology (KRIBB), Daejeon, 34141, Republic of Korea.
*** Corresponding author. Laboratory Animal Resource Center, Korea Research Institute of Bioscience and Biotechnology (KRIBB), Daejeon, 34141, Republic of Korea.
E-mail addresses: sglee@kribb.re.kr (S.-G. Lee), coccs99@kribb.re.kr (J.H. Hwang), dhlee@kribb.re.kr (D.-H. Lee).

https://doi.org/10.1016/j.bios.2020.112523
Received 16 June 2020; Received in revised form 5 August 2020; Accepted 17 August 2020
Available online 20 August 2020

gut inflammation (Archer et al., 2012; Courbet et al., 2015; Daeffler et al., 2017; McKay et al., 2018; Riglar et al., 2017).

A typical response to gut inflammation is the generation of reactive oxygen species (ROS) and reactive nitrogen species (RNS). ROS and RNS play important roles in the anaerobic respiration of Enterobacteria in the intestine. Thiosulfate ($S_2O_3^{2-}$) and tetrathionate ($S_4O_6^{2-}$) are generated from sulfur metabolism by sulfate-reducing bacteria (SRB) in the gut during inflammation. When infected by pathogenic bacteria, such as *Salmonella enterica* serovar Typhimurium (*S. typhimurium*) or *Yersinia enterocolitica*, the host produces ROS to convert thiosulfate to tetrathionate, which can then be used by pathogenic microbes as a terminal electron acceptor (TEA) (Kamdar et al., 2016; Winter et al., 2010). Enterobacteria and SRB can utilize thiosulfate as a TEA in anaerobic respiration. Recently, as biomarkers of intestinal inflammation, thiosulfate and tetrathionate have been detected by genetic circuits using a bacterial two-component regulatory system (TCS) (Daeffler et al., 2017; Riglar et al., 2017). TCS-based genetic circuits of *Shewanella* species (Daeffler et al., 2017) and *S. typhimurium* (Riglar et al., 2017) were introduced into the probiotic strain *Escherichia coli* Nissle 1917 (EcN) and the commensal murine *E. coli* NGF-1, respectively. Their functions have been validated using the dextran sodium sulfate (DSS) mouse model via colonization in the inflamed gut.

RNS also provide Enterobacteria with TEA for anaerobic respiration (Simmonds and Rampton, 1993). Gut inflammation induces the expression of nitric oxide synthase (iNOS) at high levels and increases the production of nitric oxide (NO) (Lundberg et al., 1994; Singer et al., 1996; Stanek et al., 2008). Genetic circuits capable of detecting and responding to NO have been generated previously using the NO reduction and detoxification regulator NorR that activates the transcription of NO-detoxifying flavorubredoxin (Archer et al., 2012), as well as the nitrate-sensitive repressor NsrR that regulates the expression of genes responsible for cell protection against NO (McKay et al., 2018). However, these studies did not include *in vivo* detection using the mouse model. Moreover, NO is a transient product of RNS and is easily converted to nitrate (NO_3^-) (Dudhgaonkar et al., 2007; Saijo et al., 2010). Nitric oxide radicals (NO•) can react with superoxide radicals ($O_2^{\bullet-}$) to generate peroxynitrite ($ONOO^-$), which can then yield nitrate (Szabo et al., 2007). Nitrate is used for the anaerobic respiration of Enterobacteria as TEA. Thus, we hypothesized that nitrate can be a molecule of interest for the development of a genetic circuit that detects and responds to gut inflammation. Indeed, nitrate levels have been shown to increase in the cecal mucus layer of mice with DSS-induced colitis (Winter et al., 2013).

Here, we present a designer probiotic *E. coli* to sense and report nitrate concentration in a mouse model of colitis. We developed a probiotic strain of EcN that is programmed to sense and respond to nitrate using a genetic circuit containing the nitrate-dependent TCS of *E. coli*. We optimized the performance of the nitrate-responsive genetic circuit in EcN and validated its performance in mice with colitis. The engineered EcN detected nitrate derived from gut inflammation and reported it as a fluorescence signal in colon and fecal samples, thus indicating that our designer probiotic *E. coli* can be used as a non-invasive diagnostic of gut inflammation.

2. Material and methods

2.1. Bacterial strains, plasmids, and culture conditions

The bacterial strains and plasmids used in this study are listed in Table S1. KOD Plus Neo (Toyobo) or KOD One PCR Master Mix (Toyobo) was used for PCR amplification. The plasmids were constructed using the Gibson assembly methods (Gibson et al., 2009). *E. coli* DH5α and EcN were used for plasmid propagation and the development of genetic circuits, respectively. Oligonucleotides were obtained from Macrogen (Seoul, Korea) and are listed in Table S2. Sanger sequencing (Macrogen) was used to verify the sequences of constructed plasmids. Bacterial cells were grown in lysogeny broth (LB) supplemented with the appropriate antibiotics at 37 °C. All reagents used in this study were of analytical grade and were purchased from Sigma-Aldrich.

2.2. Construction of genetic circuit

The genes encoding NarX, NarL, and P_{yeaR} promoter were amplified from the genomic DNA of *E. coli* K-12 MG1655. The superfolder green fluorescent protein (*sfgfp*) gene, the Biobrick ribosome binding site (RBS, BBa_B0034), and the Anderson promoter (BBa_J23114) were amplified from the CL-GESS plasmid (Yeom et al., 2018). RBS (BBa_B0034) was introduced between the *narX* and the BBa_J23114 promoter by annealing oligonucleotides. For the simple and efficient replacement of BBa_J23114 with various constitutive promoters regulating the expression of *narX* and *narL* genes, we designed the primers for amplifying BBa_J23114 flanked with prefix and suffix sequences harboring XbaI and NotI restriction enzyme sites. To optimize the intracellular expression of *narX* and *narL* genes, BBa_J23114 was replaced with various constitutive promoters from the Anderson promoter library (Kelly et al., 2009). The plasmid backbone was prepared by digesting the pSEVA131-J23114-NPG plasmid with XbaI and NotI-HF restriction enzymes. The PCR-amplified Anderson promoters constructed by annealing oligonucleotides and the digested pSEVA131-J23114-NPG plasmid were assembled using the Gibson Assembly Master Mix (New England Biolabs, Ipswich, MA). Single point mutation of the *narX* variants with H399A, H513Q, and N509D were constructed through overlap PCR.

2.3. Generation of E. coli mutant strains

The λ-Red recombination method (Datsenko and Wanner, 2000) was used to knock out the endogenous genes (*narX* and *narL*) from EcN. EcN cells containing the pKD46 plasmid were transformed using a linear PCR product containing a kanamycin resistance cassette and the homology arms amplified from the template plasmid pKD4 using NarD-F and NarD-R primers. The resulting colonies were selected on LB agar plates with 50 μg/mL kanamycin and then confirmed through colony PCR using NarV-F and NarV-R primers. The kanamycin resistance gene was removed from the EcN chromosome using the pCP20 plasmid that was then cured by growing the cells at 42 °C. The *narX-narL* deletion mutant was confirmed through Sanger sequencing of the PCR products.

2.4. Performance of genetic circuit under aerobic conditions

EcN cells harboring the genetic circuits were grown in 3 mL of LB supplemented with 100 μg/mL ampicillin at 37 °C with shaking at 200 rpm overnight. Overnight cultures were diluted 1000-fold with fresh 3 mL of M9 glycerol medium, supplemented with 100 μg/mL ampicillin, 1x M9 salts, 0.4% v/v glycerol, 0.2% w/v casamino acids, 2 mM $MgSO_4$, and 100 μM $CaCl_2$, and incubated at 37 °C for 3 h with shaking at 200 rpm. After 3 h, the cell suspensions were diluted to 1:100 with the M9 medium and loaded into a well of a black-walled 96-well polystyrene microplate to a final volume of 198 μL/well. The loaded cultures were then incubated with 2 μL of the appropriate inducers for 6 h at 37 °C with shaking at 800 rpm. Measurements of optical density at 600 nm (OD_{600}) and fluorescence using an excitation and emission wavelength at 488 and 515 nm, respectively, were performed using a multi-label microplate reader (PerkinElmer, Waltham, MA, USA). To measure the fluorescence at a single-cell level, a FACS Calibur flow cytometer (BD Bioscience, Franklin Lakes, NJ) was used. The resulting cultures were sampled and diluted to 1:20 with 1 mL of filter-sterilized phosphate-buffered saline (PBS). Each diluted sample was used to acquire approximately 10,000 events at a low flow rate with a FL1 gain of 650. The cell populations were gated based on the distributions of forward scatter (FSC) and side scatter (SSC) obtained from wild-type (WT) EcN cells. The WT EcN cells were used as the negative control (no fluorescence), and fluorescence data obtained from gated cells were analyzed

using the Flow Jo program (Flow Jo, LLC).

2.5. Performance of genetic circuit under anaerobic conditions

M9 mucin broth was used with some modifications (Winter et al., 2013; Zhu et al., 2018). The EcN cells with the nitrate-responsive genetic circuit were grown in 3 mL of M9 glycerol broth supplemented with 100 μg/mL ampicillin with shaking at 200 rpm at 37 °C overnight. The cultured cells were diluted to 1:100 in 15 mL serum bottle containing 3 mL of M9 mucin broth, supplemented with 100 μg/mL ampicillin, 1x M9 salts, 0.5% w/v mucin from porcine stomach Type II, 0.2% w/v casamino acids, 2 mM $MgSO_4$, and 100 μM $CaCl_2$ equilibrated in anaerobic conditions. The diluted cells were incubated anaerobically with appropriate inducers at 37 °C for 6 h. After 6 h, 1 mL of the cells incubated with the inducers were centrifuged at 13,000 rpm for 3 min at 4 °C and washed with PBS containing 1 mg/mL chloramphenicol as a translational inhibitor. After re-suspension in PBS containing 1 mg/mL chloramphenicol, the cells were incubated at 37 °C in a water bath for 1 h to allow the maturation of fluorophores and were used as a sample for fluorescence analysis via flow cytometry. For fluorescence measurements, 50 μL of cells were diluted to 1:20 with 1 mL of PBS containing 1 mg/mL chloramphenicol and were analyzed. For the ligand specificity analysis of the nitrate biosensor, appropriate electron acceptors were used as described previously (Daeffler et al., 2017) including sulfate, sulfite, dimethyl sulfoxide (DMSO), nitrate, fumarate, trimethylamine *N*-oxide (TMAO), tetrathionate, and thiosulfate.

2.6. Fluorescence microscopy analysis

The bacterial cultures were mounted on a glass microscope slide and covered with a coverslip. The prepared samples were visualized using the 630x objective on a Zeiss LSM 5 Live confocal laser microscope (Carl Zeiss, Germany) equipped with a green fluorescence filter (excitation wavelength at 488 nm).

2.7. Preparation of EcN strains for in vivo study

EcN cells carrying two plasmids, pSEVA131-J23113-NPG and pAWP89-dTomato (Addgene # 61264) (Puri et al., 2015), were inoculated in 5 mL of LB liquid medium, containing 100 μg/mL ampicillin and 25 μg/mL kanamycin, in a 50-mL culture tube at 37 °C overnight with shaking at 200 rpm. The cultured cells were diluted 100-fold in 200 mL of fresh LB liquid medium containing 100 μg/mL ampicillin and 25 μg/mL kanamycin in two 1-L baffled flasks and grown at 37 °C with shaking at 200 rpm until an OD_{600nm} of ~0.5 was reached. Following incubation, the cells were pooled and pelleted by centrifugation at 3000 rpm for 20 min at 4 °C, concentrated 25-fold in 15% w/v glycerol, and stored at −80 °C for subsequent *in vivo* experiments.

2.8. Establishment of the DSS colitis model

Mice were housed at a regulated temperature (20–22 °C) on a 12:12 h light:dark schedule, with free access to food and water under specific pathogen-free conditions. All experiments were approved by the Institutional Animal Care and Use Committee of the Korea Research Institute of Bioscience and Biotechnology (KRIBB-AEC-19229). Male mice (9- to 10-weeks old) were randomly divided into six groups ($n = 5$ per group), and acute colitis was induced through 2% w/v DSS administration (MW = 36,000–50,000; MP Biomedicals) in drinking water (*ad libitum*) for 5 days. To collect the fecal samples from the groups of mice housed separately, cages were replaced before the mice were orally gavaged with engineered EcN cells. On the final day of DSS treatment, we orally inoculated the mice with 1×10^9 CFU of EcN cells harboring the nitrate-responsive genetic circuit prepared in filter-sterilized PBS via intragastric gavage. After 6 h of oral inoculation of EcN cells, the EcN cells were recovered from the fecal samples collected from each cage and from euthanized mice by flushing luminal contents from the excised colons with PBS. Fecal samples and colon effluents were collected for fluorescence-based analysis via flow cytometry.

2.9. Preparation of colon and fecal samples for flow cytometry analysis

The luminal contents extracted by scraping from the colon and fecal samples were homogenized in 1 mL of sterilized PBS containing 1 mg/mL chloramphenicol via vortex mixing for ~5 min in 2-mL microtubes. The homogenized samples were filtered (5 μm; Millex-SV, Millipore Corporation, Bedford, Mass) to exclude large particles and debris. The remaining bacterial cells in the filter membrane were also flushed with 1 mL of PBS containing 1 mg/mL chloramphenicol. The filtered fluid was incubated at 37 °C in a water bath for 1 h to allow the maturation of fluorophores and was then used as a sample for fluorescence analysis. For the quantification of GFP fluorescence, cell populations were gated using thresholds set by dTomato fluorescence and the FSC/SSC profile of WT EcN cells. Flow cytometry was used to measure GFP-positive cells as described previously (Daeffler et al., 2017).

2.10. Histopathology

Mouse colon tissue was fixed in 10% neutral-buffered formalin, embedded in paraffin, and cut to 5 μm-thick sections. The colon sections were deparaffinized, rehydrated, and stained with hematoxylin and eosin (H&E) according to a standard protocol. Blinded scoring of tissue injury was performed using a light microscope. Colonic damage was determined using a histopathological scoring system as previously described (Hwang et al., 2019).

2.11. Measurements of nitrate concentration in colon samples

Colon tissues were homogenized in cold PBS (pH 7.4) and centrifuged at 10,000 rpm for 20 min. The supernatant was filtered using a 10 kDa molecular weight cut-off system (Merck, NJ, USA). Tissue nitrate was measured using a Cayman's nitrate/nitrite colorimetric assay kit (Cayman chemical, MI, USA) according to the manufacturer's protocol. Nitrate concentration was normalized against tissue weight.

2.12. In vivo detection of EcN mutants

To determine the distribution of EcN mutants, colon tissues mice that were treated with DSS for 3 days were embedded in a frozen section compound (Leica Microsystems, Germany), cut to 8 μm-thick sections, and dried at 25 °C for 2 h. The frozen colon sections were fixed in 4% paraformaldehyde and stained with 4′,6-diamidino-2-phenylindole (DAPI). The sections were washed, mounted, and imaged using a laser-scanning confocal microscope (Nikon, NY, USA).

2.13. Designing a genetic circuit with boolean AND logic gate

For the construction of a Boolean AND logic gate in one plasmid, bioparts composing the AND logic gates were generated from pSEVA131-J23114-NPG, pKD182 (Addgene #90952) (Daeffler et al., 2017), and pKD184 (Addgene #90953) plasmids as the linear fragments (Daeffler et al., 2017) and cloned through Gibson Assembly. Single point mutation of the *thsS* variant with L547T was constructed using overlap PCR for tuning the detection thresholds of the thiosulfate biosensor as previously described (Landry et al., 2018). For the pSEVA131-AND plasmid, the constitutively expressed *narX* and *narL* genes in the reverse orientation were activated in the presence of nitrate. Phosphorylated NarL regulator protein controls the expression of *thsS* (L547T) and *thsR* genes in the forward orientation by modulating the transcription of the P_{yeaR} promoter. The expressed *thsS*(L547T) and *thsR* genes activate the expression of the *sfgfp* gene under the control of the P_{phsA} promoter in the presence of thiosulfate.

2.14. Characterization of the boolean AND logic gate

The EcN strain harboring the AND logic circuit was inoculated into LB medium. After overnight growth at 37 °C with shaking, the bacterial cultures were used to characterize the AND logic gates induced via appropriate combinations of sodium nitrate and/or sodium thiosulfate pentahydrate.

2.15. Transfer function modeling and parameter estimation

All transfer function data were fit to an activating Hill equation (eq. (1)) using the SigmaPlot package,

$$y = low + \frac{(high - low) \times x^n}{k_{1/2}{}^n + x^n} \quad (1)$$

where y is the normalized fluorescence (Fluorescence/OD_{600}) measurement; *low* is the normalized fluorescence at the basal expression level; *high* is the maximum normalized fluorescence due to induction; x is the inducer concentration; $K_{1/2}$ is the Hill constant (that is, the concentration of inducer that provokes half-maximal normalized fluorescence); and n is the Hill coefficient.

2.16. Statistical analysis

Data are expressed as the mean ± standard deviation (SD).

3. Results and discussion

3.1. Design and development of nitrate-responsive genetic circuits

Gut nitrate levels increase during inflammation due to iNOS expression (Winter et al., 2013). The nitrate/nitrite redox couple shows a higher redox potential than other redox couples (DMSO/DMS, TMAO/TMA), which confers the preferred respiratory TEA to nitrate for *E. coli* growth under anaerobic conditions (Fig. 1A) (Neidhardt and Curtiss, 1996). Instead of using previously reported regulators, NorR (Archer et al., 2012) and NsrR (McKay et al., 2018), which could detect NO, we built nitrate-responsive genetic circuits using nitrate reductase (Nar) TCS, NarX-NarL (NarXL), which is involved in the anaerobic respiration of *E. coli* (Rabin and Stewart, 1992; Stewart, 2003).

We first constructed a single plasmid containing both the *narXL* genes and a sfGFP fluorescent reporter, which is regulated by the NarL responsive promoter, P_{yeaR} (Fig. 1B) (Lin et al., 2007). *narXL* genes are expressed by a constitutive promoter in the direction opposite to the transcription of *sfgfp* gene. We generated two kinds of genetic circuits using two backbone plasmids with different copy numbers, i.e., pSEVA131-J23114-NPG (pBBR1 medium copy number origin) and pSEVA141-J23114-NPG (ColE1 high copy number origin). To examine the performance of the two nitrate-responsive genetic circuits, WT EcN cells containing the individual genetic circuits were grown in M9 minimal medium supplemented with different nitrate concentrations (0–10 mM) (Fig. 1C). EcN cells harboring pSEVA131-J23114-NPG clearly responded to nitrate induction and showed 4-fold fluorescence increase relative to the uninduced control (Fig. 1C, lower panel), whereas WT EcN cells transformed with pSEVA141-J23114-NPG showed no significant difference among all nitrate concentrations (Fig. 1C, upper panel). Therefore, we chose the medium copy nitrate-responsive genetic circuit for subsequent experiments.

Next, we systematically tuned the expression of *narXL* genes to improve the sensitivity of the nitrate-responsive genetic circuit using well-characterized Anderson promoters (J23113, J23117, J23114, J23105, J23106; shown in order of increasing activity). The performance of individual genetic circuits was evaluated using transfer function parameters and the limit of detection (LoD) (Bergstrom et al., 2010). As the strength of the Anderson promoter increased, both LoD and dynamic detection range (DDR) decreased (Fig. S1 and S2). WT EcN cells containing the nitrate-responsive genetic circuit under the control of the weakest promoter (J23113) sensed 9.8 μM nitrate, which was 8-times lower than the LoD of the nitrate-responsive genetic circuit with the strongest promoter (J23106) (Fig. 1D, upper panel and S1). Moreover, the DDR of the J23113-nitrate-responsive genetic circuit was 4-times higher than that of the J23106-nitrate-responsive genetic circuit.

We then removed the endogenous *narXL* operon from the WT EcN chromosome to avoid the cross-regulation of NarXL expressed in the genetic circuit plasmids introduced into WT EcN, which resulted in the EcN*ΔnarXL* strain. The responses of EcN*ΔnarXL,* with nitrate-responsive genetic circuit containing Anderson promoters of different strengths, to various nitrate concentrations were determined (Fig. 1D, lower panel and S2). Like WT EcN, the EcN*ΔnarXL* strain showed lower LoD and higher DDR values as the strength of the promoter decreased. The best nitrate sensor strain of EcN*ΔnarXL* (J23113 promoter) showed an LoD of 4.9 μM, which was 2-times lower than that of WT EcN containing the same construct, and the EcN*ΔnarXL* strain exhibited 1.25-times higher DDR than did WT EcN (Fig. 1D, lower panel).

Finally, we generated a null mutant of NarX to confirm whether the fluorescence output of the nitrate-responsive genetic circuits is caused by the detection of exogenously added nitrate. NarX sensory histidine kinase is required for activation of the NarL response transcriptional regulator to control anaerobic respiratory gene expression in *E. coli* (Cavicchioli et al., 1995). We introduced three individual point mutations into NarX, which resulted in three NarX variants, namely, NarX-H399A, NarX-H513Q, and NarX-N509D. Three nitrate-responsive genetic circuits with NarX variants lost their responses to nitrate concentrations ranging from 0–10 mM (Fig. 1E, upper panel and S3),indicating that the nitrate-responsive genetic circuits constructed with WT NarX responded to the presence of nitrate by triggering the transcription of the *sfgfp* gene in a phosphorylation-dependent manner. To explore the fluorescence induction pattern of EcN*ΔnarXL* (J23113 promoter), fluorescence was determined using a flow cytometer in the presence of various nitrate concentrations (0–10 mM) (Fig. 1E). At each nitrate concentration, the majority of individual cells showed fluorescence, indicating that the individual cell responses reflected the population-averaged behavior measured by the fluorometer (Fig. 1E, left panel). In addition, we confirmed the LoD (9.8 μM) value of EcN*ΔnarXL* (J23113 promoter) (Fig. 1E, right lower panel).

To visualize the activation of the nitrate-responsive genetic circuits, EcN*ΔnarXL* (J23113 promoter) cells induced by 156 μM nitrate were observed using confocal fluorescence microscopy (Fig. 1F), the results of which were consistent with our flow cytometry analysis. As expected, NarX-H399A null mutant showed no response to the presence of nitrate in both flow cytometry analysis (Fig. 1E, upper panel) and confocal fluorescence microscopy (Fig. 1F, left panel).

3.2. Sensitivity and specificity of nitrate-responsive genetic circuits

The conditions of the intestinal environment where the nitrate-responsive genetic circuit will be implemented are very different from the experimental conditions where they were validated. Thus, we mimicked the intestinal environments through the addition of mucin into the culture medium and the culture of EcN*ΔnarXL* cells under anaerobic conditions. EcN*ΔnarXL* strain with NarX-H399A and glycerol were used as controls for strain and medium, respectively. In the glycerol medium, EcN*ΔnarXL* cells with NarXL grown in the presence of nitrate showed 12-fold higher fluorescence than that obtained in the absence of nitrate (Fig. 2A). In the mucin medium, 6.5-fold higher fluorescence was observed in the presence of nitrate. EcN with NarX-H399A showed no fluorescence activity regardless of the kind of medium and nitrate concentration (Fig. 2A). These results show that the nitrate-responsive genetic circuits work effectively under intestine-like anaerobic conditions.

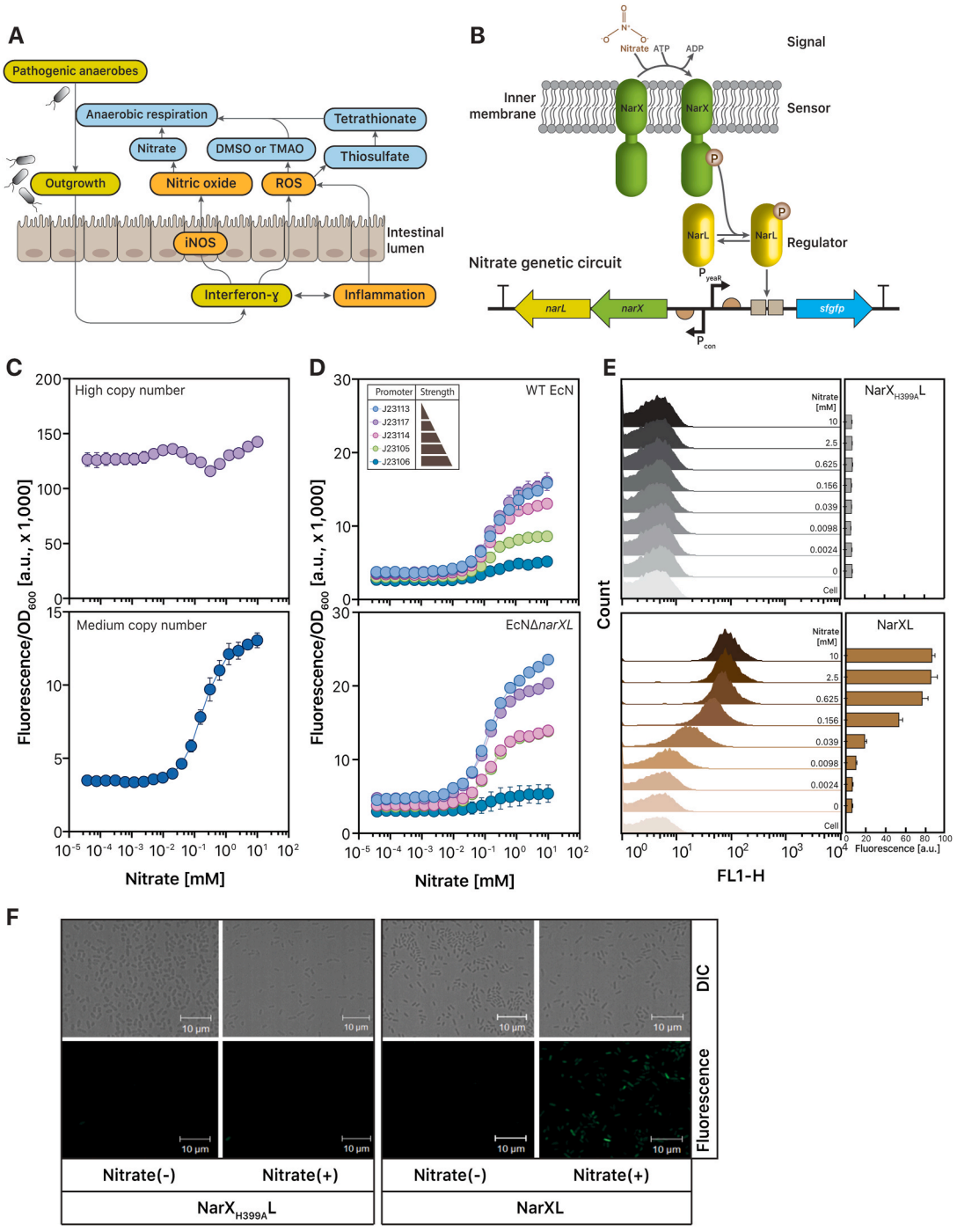

Fig. 1. Schematic representation and characterization of the nitrate-responsive genetic circuits. (A) Correlation between increased production of nitrate, reactive oxygen species (ROS), and alternative electron acceptors, and intestinal inflammation. Interferon-ɣ stimulated by inflammation generates nitrate and ROS that are used as alternative electron acceptors for pathogenic bacteria outgrowth through anaerobic respiration. Pathogenic bacteria also utilize dimethyl sulfoxide (DMSO), trimethylamine N-oxide (TMAO), thiosulfate, or tetrathionate as terminal electron acceptors. Increased nitrate production by inducible NO synthase (iNOS) during intestinal inflammation indicates that nitrate can be a biomarker for gut inflammation. (B) Design and development of the nitrate-responsive genetic circuit. In the presence of nitrate, constitutively expressed NarX becomes phosphorylated, thereby phosphorylating NarL, which drives the expression of the *sfgfp* reporter gene through the *yeaR* promoter. (C) Comparison of dose-response curves generated from the nitrate-responsive genetic circuit under the control of the indicated origin of replication (ColE1 high copy number or pBBR1 medium copy number) analyzed using a microplate reader ($n = 3$ biological repeats; error bars represent standard deviation, SD). (D) Characterization of a set of constitutive promoters having different transcriptional strengths to express *narXL* genes in WT EcN and EcNΔ*narXL* (that is, *narXL* genes were knocked out in the chromosome) in response to nitrate concentrations ($n = 3$ biological repeats, error bars represent SD). (E) Reporter sfGFP signal measured using flow cytometry. The responsiveness of $NarX_{H399A}L$ and NarXL was analyzed. Fluorescence histograms depict the homogeneous expression of the reporter *sfgfp* gene under all nitrate concentrations for NarXL. For each measurement, 10,000 events were collected with a FL1 gain of 650. WT EcN cells do not contain fluorescent plasmid and were used as the control. Representative mean and SD values of fluorescence were quantified using flow cytometry under increasing nitrate concentrations as indicated on the right panel of each histogram ($n = 3$ biological repeats; error bars represent SD). (F) Microscopic visualization of the EcNΔ*narXL* cells with $NarX_{H399A}L$ or NarXL in the absence (Nitrate -) and presence of nitrate (Nitrate +, 156 μM) using differential interference contrast (DIC) and confocal fluorescence microscopy.

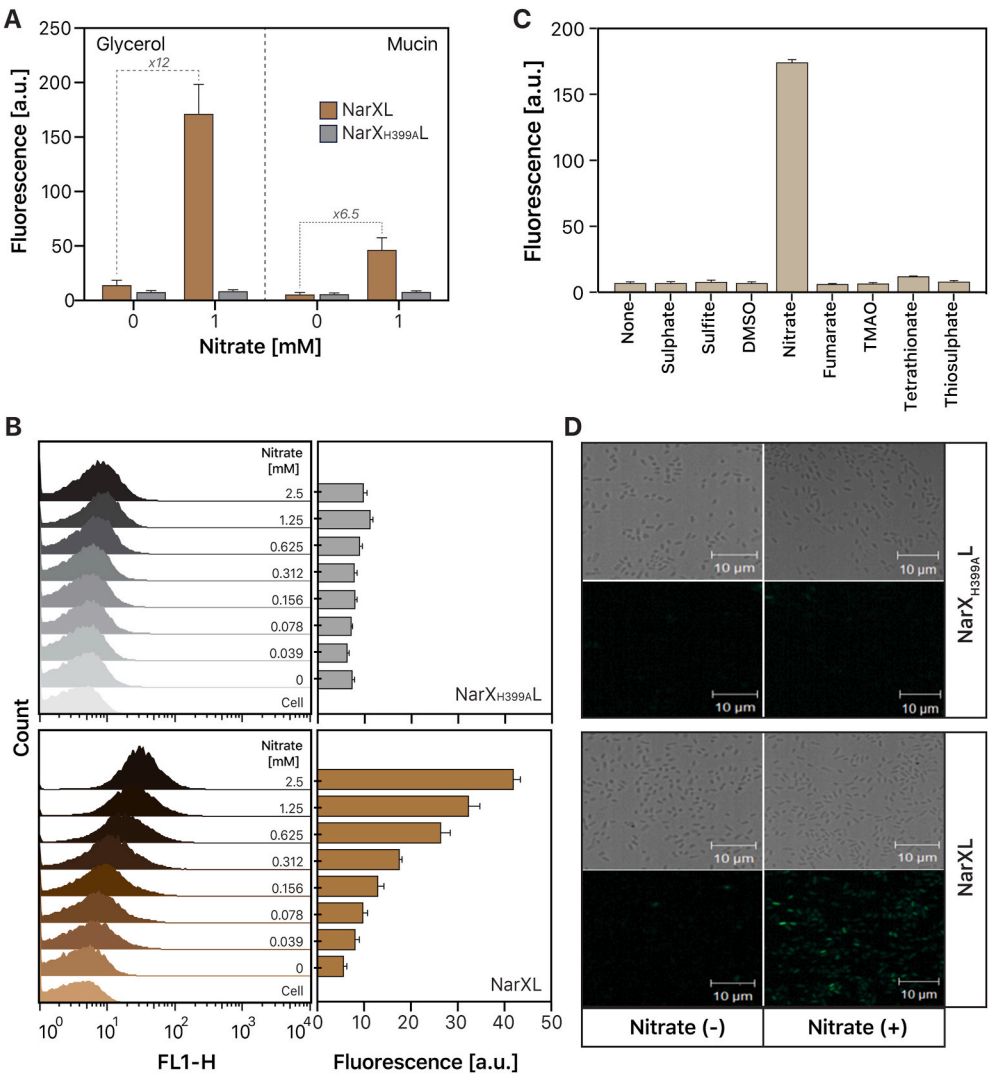

Fig. 2. Evaluation of the functionality and ligand-specificity of the nitrate-responsive genetic circuit. (A) Mean fluorescence values of the nitrate-responsive genetic circuits in glycerol and mucin media under anaerobic conditions and in the presence and absence of nitrate as measured using flow cytometry (n = 3 biological repeats; error bars represent SD). (B) Evaluation of the *sfgfp* reporter gene whose expression is induced by nitrate at the indicated concentrations in mucin media under anaerobic conditions. GFP fluorescence of the EcNΔ*narXL* cells with $NarX_{H399A}L$ or NarXL was analyzed using flow cytometry. The histograms depict homogeneous cell populations and right shift of fluorescence at increasing nitrate concentrations only in the NarXL. For each measurement, 10,000 events were collected with a FL1 gain of 650. WT EcN cells did not contain the fluorescent plasmid and were considered as no-fluorescence populations. Representative mean and SD values of the EcNΔ*narXL* cells with $NarX_{H399A}L$ or NarXL were obtained through flow cytometry at increasing nitrate concentrations as indicated on the right panel of each histogram (n = 3 biological repeats; error bars represent SD). (C) Ligand-specificity of the nitrate-responsive genetic circuit was determined through the analysis of the sfGFP reporter using flow cytometer without (none) or with the indicated terminal electron acceptors (TEAs) at final concentrations of 10 mM under anaerobic conditions in mucin media (n = 3 biological repeats; error bars represent SD). (D) Microscopic observation of the EcNΔ*narXL* cells with $NarX_{H399A}L$ or NarXL in the absence (Nitrate -) and presence of nitrate (Nitrate +, 625 μM) in mucin media under anaerobic conditions using DIC and confocal fluorescence microscopy.

To monitor the anaerobic response of the genetic circuit to nitrate at the single-cell level, we performed flow cytometry analysis using different nitrate concentrations (0–2.5 mM). The EcNΔ*narXL* cells with NarXL were grown in the medium supplemented with mucin and various amounts of nitrate under anaerobic condition. As expected, the EcNΔ*narXL* strain with NarXL responded in a dose-dependent manner to nitrate (Fig. 2B, lower panel). In addition, the LoD of the nitrate-responsive genetic circuit was 39 μM nitrate. These results were corroborated using confocal fluorescence microscopy (Fig. 2D, lower panel). The EcNΔ*narXL* strain with NarX-H399A showed no fluorescence activity in both flow cytometry (Fig. 2B, upper panel) and confocal microscopy (Fig. 2D, upper panel).

We then examined the specificity of the nitrate-responsive genetic circuit against a wide range of TEAs, which are also generated from an inflamed mammalian intestine (Simmonds and Rampton, 1993). Eight alternative TEAs were tested, including sulfate, sulfite, dimethyl sulfoxide (DMSO), nitrate, fumarate, trimethylamine *N*-oxide (TMAO), tetrathionate, and thiosulfate, at a concentration of 10 mM, which is well above that expected in the gut. Among them, nitrate is known as a TEA for the commensal bacterium *E. coli*, increasing *E. coli*'s growth compared with other competing microbes (Winter et al., 2013). The nitrate-responsive genetic circuit showed the highest fluorescence intensity in the presence of nitrate (Fig. 2C). Other TEAs showed similar fluorescence activity as the negative control, which indicates that the nitrate-responsive genetic circuit did not sense any of these ligands.

3.3. Nitrate-responsive genetic circuit in DSS-induced colitis mouse model

DSS, a colitogenic compound, is used to induce the widely used colitis mouse model as it exhibits anticoagulant effects on the intestinal epithelial cells of mice (Eichele and Kharbanda, 2017). In this study, gut inflammation in mice was induced similarly, and its progress was monitored by determining changes in the body weight, levels of pro-inflammatory cytokine in the plasma, pathology, and histologic scoring, which were compared with those in healthy mice (at Day 0) for 5 days (Fig. 3A). Body weight was reduced (Fig. 3B), and IL-6 levels in the plasma were strongly increased (Fig. 3C) four days after DSS administration. DSS administration further induced inflammation-associated changes in the colon mucus layer (Fig. 3D and E). Overall, we confirmed that gut inflammation was gradually worsened by DSS treatment in C57BL/6 mice.

Nitrate levels reportedly increased during an inflammatory response in the gut of DSS colitis Wistar rats (Saijo et al., 2010). A memory genetic circuit that detects tetrathionate, another biomarker for inflammation, responded in 129X1/SvJ mice, but not in BALB/c or C57BL/6 mice (Riglar et al., 2017). We therefore determined the nitrate concentrations during gut inflammation, because we employed a different rodent model, C57BL/6, in this study. Nitrate concentrations increased gradually over time after DSS treatment, reaching a maximum of 723.38 ± 107.8 μM per g of tissue on day 4, but slightly decreased to 610.29 ± 83 μM per g of tissue on day 5 (Fig. 3F). The nitrate concentrations

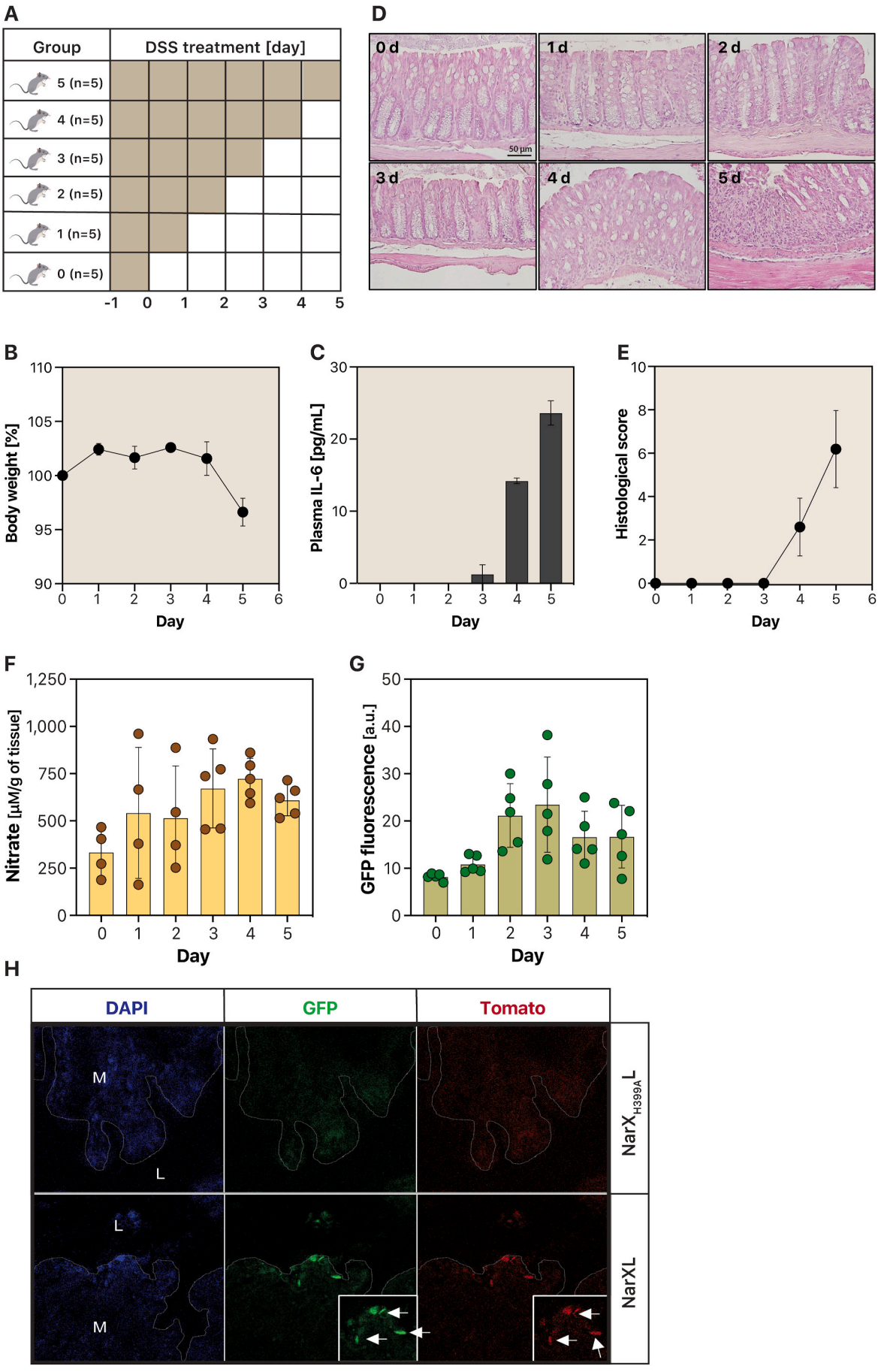

(caption on next page)

Fig. 3. Influence of DSS treatment on intestinal inflammation, nitrate concentrations, and normalized GFP levels. (A) Schematic representation of the experimental design for the colitis mouse model used in this study. Male C57BL/6 mice (9- to 10-weeks old) were given water with or without 2% w/v DSS and divided into groups according to length of DSS treatment. Disease assessment was conducted on the last day of DSS treatment ($n = 5$ per group). (B) Mouse body weight during the progression of intestinal inflammation ($n = 5$ per group). (C) IL-6 levels in plasma samples ($n = 5$ per group). (D) Representative pictures of hematoxylin and eosin (H&E)-stained colonic sections. Scale bar, 50 μm. (E) Histological score for the colon ($n = 5$ per group). Unless otherwise indicated, data are shown as the geometric mean and SD. (F) Nitrate concentration in mouse colon tissues according to length of DDS treatment (Day 0–5). Dots indicate individual mice, whereas bars indicate normalized mean nitrate concentration. (G) Normalized GFP levels in the colon samples of mice gavaged with engineered EcN strain. Mice were divided into groups according to the length of DSS treatment ($n = 5$ per group). They were gavaged with 10^9 of EcN cells harboring the nitrate-responsive genetic circuit, and colon samples were collected, processed, and analyzed 6 h after bacterial administration. Dots indicate individual mice, whereas bars indicate normalized mean fluorescence. (H) Fluorescence microscopic visualization of colon sections of mice administered EcN strains with NarXL or $NarX_{H399A}L$. Arrows indicate administered EcN strains constitutively expressing dTomato and the sfGFP reporter protein induced by nitrate concentrations in the inflamed large intestine. Abbreviations: M, mucosa; L, lumen.

measured were sufficient to be sensed or responded to by the genetic circuit under both aerobic and anaerobic conditions (Figs. 1 and 2).

Given this, we probed the ability of the nitrate-responsive genetic circuits to sense and respond to nitrate generated from DSS colitis C57BL/6 mouse model (Fig. 3G). To this end, we measured the fluorescence intensity and observed fluorescence-activated EcN cells under fluorescence microscopy. To distinguish our engineered EcN cells from the native gut microbiota and particles, we used a dTomato expression plasmid (pAWP89-dTomato) constitutively expressing dTomato. Three days after DSS treatment, the fluorescence activity of the engineered EcN cells increased compared with that of the control (Day 0) (Fig. 3G and S5). Furthermore, we directly determined the fluorescence activity of the colonized EcN cells in the mucus layer and found that they exhibited the red fluorescence activity of dTomato and the green fluorescence activity of sfGFP (Fig. 3H). The fluorescence output profiles of the intestinal contents of DSS-induced colitis mice correlated well with the pattern of increased nitrate levels determined from inflamed colons (Fig. 3F and G). This confirms that the nitrate-responsive genetic circuits are activated by a host-derived nitrate in the inflamed large intestine of the C57BL/6 mouse model. In addition, the elevated levels of nitrate during inflammatory response can be a biomarker for colitis. To our knowledge, this is the first study to generate an EcN strain harboring a nitrate-responsive genetic circuit as a biosensor for intestinal inflammation in a DSS colitis mouse model. Moreover, we monitored the nitrate concentrations by more detained time-resolved assays and used flow cytometry to analyze complex colon and fecal samples to determine the sfGFP fluorescence of the EcN cells. Flow cytometry analysis allows measurement of EcN populations at a single-cell level, which provides more information on the physiologically relevant response of the nitrate-responsive genetic circuit in the gut environment.

3.4. Genetic circuit detects both nitrate and thiosulfate using boolean AND logic gate

Multiple biomarkers improve the performance and robustness of synthetic genetic circuits in clinical samples (Courbet et al., 2015; Giljohann and Mirkin, 2009). Thiosulfate has been detected by a genetic circuit as a biomarker of gut inflammation (Daeffler et al., 2017). To improve the specificity and reduce false positives for diagnosis, we designed and engineered the genetic circuits to express the reporter gene only when both biomarkers for RNS and ROS are present (Fig. 4A). We constructed the orthogonal Boolean AND logic gate using the nitrate-responsive genetic circuit we developed and the thiosulfate genetic circuit previously developed with TCS composed of the ThsS-ThsR of the marine bacterium *Shewanella halifaxensis* (Landry et al., 2018). To construct and optimize the Boolean AND logic gate, we first designed a thiosulfate biosensor in one-plasmid with a pBBR1 origin of replication and optimized its transcriptional strength for the expression of the ThsS (L547T)-ThsR (Fig. S4). Then, we confirmed the functionality of the two-input AND logic gates that responded when both nitrate and thiosulfate are present. We analyzed their performance using the normalized fluorescence output (Fig. 4B). The AND logic gate was repressed in response to null-input conditions, and no significant difference was observed between conditions with the absence of both biomarkers and with the presence of only one biomarker (nitrate or thiosulfate). As expected, the logic AND gate operated correctly in response to different

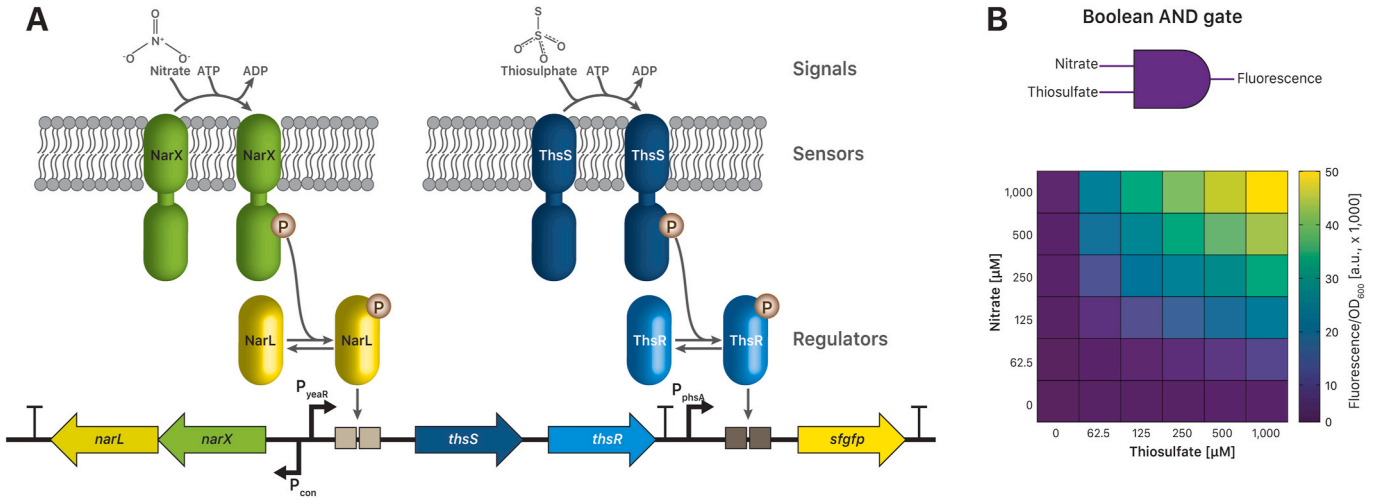

Fig. 4. Development and characterization of the Boolean AND logic gate. (A) Schematic of AND logic gate that uses nitrate and thiosulfate genetic circuits. In the presence of nitrate, constitutively expressed NarXL proteins are phosphorylated and activates the expression of ThsS(L547T)R proteins through the *yeaR* promoter. When thiosulfate is present, expressed ThsS(L547T)R proteins are phosphorylated and activate the expression of the sfGFP reporter protein via the *phsA* promoter. (B) Performance of AND logic gate at various combinations of nitrate and thiosulfate. *X*-axis and *Y*-axis indicate the concentrations of thiosulfate and nitrate, respectively. Color bar (lower right) indicates fluorescence/OD_{600} [a.u., x 1000]. Heatmap indicates responsiveness of each AND logic gate at different combinations of nitrate and thiosulfate. Heatmap values represent the mean of two biological replicates.

combinations of nitrate and thiosulfate as the inputs with high fold-change between ON and OFF states. An ON/OFF ratio of 17-fold was observed in the normalized fluorescence output between the null-input conditions and the highest input concentrations (Fig. 4B).

In this study, inflammation mouse model through DSS administration was used to increase the thiosulfate level by H_2S detoxification. However, thiosulfate can be produced from DSS through sulfur metabolism by gut microbiota. The nitrate-responsive genetic circuit we presented here is free from thiosulfate cross-regulation and functions in both aerobic and anaerobic conditions. These advantages resulted in the specificity of the Boolean AND logic gate, i.e., responding only when both nitrate and thiosulfate were present. This reduces false positive results during diagnosis. On the off-chance that dietary nitrate elevates the nitrate level in the large intestine, the nitrate-responsive biosensor may yield high false positives in identifying the inflammation. However, this can be overcome by the biosensor sensing both nitrate and thiosulfate simultaneously because it responds only when both nitrate and thiosulfate are present in the colon.

4. Conclusions

Our study demonstrated that a probiotic microbe can be engineered to sense and respond non-invasively to a biomarker of gut inflammation. The nitrate-responsive biosensor was generated using the bacterial two-component system, and its performance was optimized *in vitro*. The probiotic microbe equipped with the nitrate-responsive biosensor can sense elevated nitrate levels during gut inflammation in mice. Using the Boolean AND gate, we created a genetically encoded biosensor for simultaneous sensing of both inflammation biomarkers, nitrate and thiosulfate, thus increasing the tool's specificity for diagnosing gut inflammation. The nitrate-responsive biosensors will enable new approaches for non-invasive diagnostics of inflammation-associated diseases. Besides its diagnostic purpose, the nitrate biosensor could also be used for therapeutics by replacing the reporter *sfgfp* gene with an anti-inflammatory gene, thus resulting in the development of anti-inflammatory devices based on the engineered probiotics. Furthermore, the two-input AND logic gate has numerous potentials as a non-invasive diagnostic tool, as it specifically detects the two biomarkers relevant to intestinal inflammation. By combining diverse synthetic Boolean logic gates with nitrate and thiosulfate biosensors, the applicability of our developed genetic circuit can be increased. However, further studies should be conducted to improve the performance of the AND logic gate and to characterize various experimental conditions.

Funding

This work was supported by the Bio & Medical Technology Development Program [grant number 2018M3A 9H3024746] of the National Research Foundation funded by the Ministry of Science and ICT of the Republic of Korea; and the KRIBB Research Initiative Program.

CRediT authorship contribution statement

Seung-Gyun Woo: Conceptualization, Methodology. **Sung-Je Moon:** Methodology. **Seong Keun Kim:** Investigation, Data curation, Formal analysis. **Tae Hyun Kim:** Methodology. **Hyun Seung Lim:** Methodology. **Gun-Hwi Yeon:** Methodology. **Bong Hyun Sung:** Methodology. **Chul-Ho Lee:** Conceptualization, Validation, Investigation. **Seung-Goo Lee:** Conceptualization, Methodology. **Jung Hwan Hwang:** Conceptualization, Methodology. **Dae-Hee Lee:** Conceptualization, Methodology.

Declaration of competing interest

The authors declare that they have no known competing financial interests or personal relationships that could have appeared to influence the work reported in this paper.

Acknowledgments

We thank Victor de Lorenzo of Centro Nacional de Biotecnología (Madrid, Spain) for providing the pSEVA plasmids.

Appendix A. Supplementary data

Supplementary data related to this article can be found at https://doi.org/10.1016/j.bios.2020.112523.

References

Archer, E.J., Robinson, A.B., Suel, G.M., 2012. Engineered E. coli that detect and respond to gut inflammation through nitric oxide sensing. ACS Synth. Biol. 1 (10), 451–457.
Belkaid, Y., Hand, Timothy W., 2014. Role of the microbiota in immunity and inflammation. Cell 157 (1), 121–141.
Bergstrom, K.S., Kissoon-Singh, V., Gibson, D.L., Ma, C., Montero, M., Sham, H.P., Ryz, N., Huang, T., Velcich, A., Finlay, B.B., Chadee, K., Vallance, B.A., 2010. Muc2 protects against lethal infectious colitis by disassociating pathogenic and commensal bacteria from the colonic mucosa. PLoS Pathog. 6 (5), e1000902.
Cavicchioli, R., Schroder, I., Constanti, M., Gunsalus, R.P., 1995. The NarX and NarQ sensor-transmitter proteins of Escherichia coli each require two conserved histidines for nitrate-dependent signal transduction to NarL. J. Bacteriol. 177 (9), 2416–2424.
Courbet, A., Endy, D., Renard, E., Molina, F., Bonnet, J., 2015. Detection of pathological biomarkers in human clinical samples via amplifying genetic switches and logic gates. Sci. Transl. Med. 7 (289), 289ra283.
Daeffler, K.N., Galley, J.D., Sheth, R.U., Ortiz-Velez, L.C., Bibb, C.O., Shroyer, N.F., Britton, R.A., Tabor, J.J., 2017. Engineering bacterial thiosulfate and tetrathionate sensors for detecting gut inflammation. Mol. Syst. Biol. 13 (4), 923.
Datsenko, K.A., Wanner, B.L., 2000. One-step inactivation of chromosomal genes in Escherichia coli K-12 using PCR products. Proc. Natl. Acad. Sci. U. S. A. 97 (12), 6640–6645.
Dudhgaonkar, S.P., Tandan, S.K., Kumar, D., Raviprakash, V., Kataria, M., 2007. Influence of simultaneous inhibition of cyclooxygenase-2 and inducible nitric oxide synthase in experimental colitis in rats. Inflammopharmacology 15 (5), 188–195.
Eichele, D.D., Kharbanda, K.K., 2017. Dextran sodium sulfate colitis murine model: an indispensable tool for advancing our understanding of inflammatory bowel diseases pathogenesis. World J. Gastroenterol. 23 (33), 6016–6029.
Fischbach, Michael A., Sonnenburg, Justin L., 2011. Eating for two: how metabolism establishes interspecies interactions in the gut. Cell Host Microbe 10 (4), 336–347.
Gibson, D.G., Young, L., Chuang, R.Y., Venter, J.C., Hutchison 3rd, C.A., Smith, H.O., 2009. Enzymatic assembly of DNA molecules up to several hundred kilobases. Nat. Methods 6 (5), 343–345.
Giljohann, D.A., Mirkin, C.A., 2009. Drivers of biodiagnostic development. Nature 462 (7272), 461–464.
Hwang, I.Y., Chang, M.W., 2020. Engineering commensal bacteria to rewire host–microbiome interactions. Curr. Opin. Biotechnol. 62, 116–122.
Hwang, J.H., Kim, T.H., Kim, Y.H., Noh, J.R., Choi, D.H., Kim, K.S., Lee, E.Y., Kim, B.C., Kim, M.H., Kim, H., Lee, T.G., Lee, J.S., Lee, C.H., 2019. Gadd45beta promotes regeneration after injury through TGFbeta-dependent restitution in experimental colitis. Exp. Mol. Med. 51 (10), 1–14.
Kamdar, K., Khakpour, S., Chen, J., Leone, V., Brulc, J., Mangatu, T., Antonopoulos, D.A., Chang, E.B., Kahn, S.A., Kirschner, B.S., Young, G., DePaolo, R.W., 2016. Genetic and metabolic signals during acute enteric bacterial infection alter the microbiota and drive progression to chronic inflammatory disease. Cell Host Microbe 19 (1), 21–31.
Kelly, J.R., Rubin, A.J., Davis, J.H., Ajo-Franklin, C.M., Cumbers, J., Czar, M.J., de Mora, K., Glieberman, A.L., Monie, D.D., Endy, D., 2009. Measuring the activity of BioBrick promoters using an in vivo reference standard. J. Biol. Eng. 3 (1), 4.
Landry, B.P., Palanki, R., Dyulgyarov, N., Hartsough, L.A., Tabor, J.J., 2018. Phosphatase activity tunes two-component system sensor detection threshold. Nat. Commun. 9 (1), 1433.
Lin, H.-Y., Bledsoe, P.J., Stewart, V., 2007. Activation of yeaR-yoaG operon transcription by the nitrate-responsive regulator NarL Is independent of oxygen- responsive Regulator Fnr in *Escherichia coli* K-12. J. Bacteriol. 189 (21), 7539.
Lundberg, J.O., Hellstrom, P.M., Lundberg, J.M., Alving, K., 1994. Greatly increased luminal nitric oxide in ulcerative colitis. Lancet 344 (8938), 1673–1674.
McKay, R., Hauk, P., Quan, D., Bentley, W.E., 2018. Development of cell-based sentinels for nitric oxide: ensuring marker expression and unimodality. ACS Synth. Biol. 7 (7), 1694–1701.
Mimee, M., Citorik, R.J., Lu, T.K., 2016. Microbiome therapeutics - advances and challenges. Adv. Drug Deliv. Rev. 105 (Pt A), 44–54.
Neidhardt, F.C., Curtiss, R., 1996. Escherichia Coli and Salmonella: Cellular and Molecular Biology. ASM Press.
Pham, H.L., Ho, C.L., Wong, A., Lee, Y.S., Chang, M.W., 2017. Applying the design-build-test paradigm in microbiome engineering. Curr. Opin. Biotechnol. 48, 85–93.
Puri, A.W., Owen, S., Chu, F., Chavkin, T., Beck, D.A.C., Kalyuzhnaya, M.G., Lidstrom, M. E., 2015. Genetic tools for the industrially promising methanotroph *Methylomicrobium buryatense*. Appl. Environ. Microbiol. 81 (5), 1775.

Rabin, R.S., Stewart, V., 1992. Either of two functionally redundant sensor proteins, NarX and NarQ, is sufficient for nitrate regulation in Escherichia coli K-12. Proc. Natl. Acad. Sci. U. S. A. 89 (18), 8419–8423.
Riglar, D.T., Giessen, T.W., Baym, M., Kerns, S.J., Niederhuber, M.J., Bronson, R.T., Kotula, J.W., Gerber, G.K., Way, J.C., Silver, P.A., 2017. Engineered bacteria can function in the mammalian gut long-term as live diagnostics of inflammation. Nat. Biotechnol. 35 (7), 653–658.
Riglar, D.T., Silver, P.A., 2018. Engineering bacteria for diagnostic and therapeutic applications. Nat. Rev. Microbiol. 16 (4), 214–225.
Saijo, F., Milsom, A.B., Bryan, N.S., Bauer, S.M., Vowinkel, T., Ivanovic, M., Andry, C., Granger, D.N., Rodriguez, J., Feelisch, M., 2010. On the dynamics of nitrite, nitrate and other biomarkers of nitric oxide production in inflammatory bowel disease. Nitric Oxide 22 (2), 155–167.
Sampson, Timothy R., Mazmanian, Sarkis K., 2015. Control of brain development, function, and behavior by the microbiome. Cell Host Microbe 17 (5), 565–576.
Simmonds, N.J., Rampton, D.S., 1993. Inflammatory bowel disease–a radical view. Gut 34 (7), 865–868.
Singer II, Kawka, D.W., Scott, S., Weidner, J.R., Mumford, R.A., Riehl, T.E., Stenson, W. F., 1996. Expression of inducible nitric oxide synthase and nitrotyrosine in colonic epithelium in inflammatory bowel disease. Gastroenterology 111 (4), 871–885.
Singh, B., Mal, G., Marotta, F., 2017. Designer probiotics: paving the way to living therapeutics. Trends Biotechnol. 35 (8), 679–682.
Stanek, A., Gadowska-Cicha, A., Gawron, K., Wielkoszynski, T., Adamek, B., Cieslar, G., Wiczkowski, A., Sieron, A., 2008. Role of nitric oxide in physiology and pathology of the gastrointestinal tract. Mini Rev. Med. Chem. 8 (14), 1549–1560.
Stewart, V., 2003. Nitrate- and nitrite-responsive sensors NarX and NarQ of proteobacteria. Biochem. Soc. Trans. 31 (1), 1–10.
Szabo, C., Ischiropoulos, H., Radi, R., 2007. Peroxynitrite: biochemistry, pathophysiology and development of therapeutics. Nat. Rev. Drug Discov. 6 (8), 662–680.
Winter, S.E., Thiennimitr, P., Winter, M.G., Butler, B.P., Huseby, D.L., Crawford, R.W., Russell, J.M., Bevins, C.L., Adams, L.G., Tsolis, R.M., Roth, J.R., Baumler, A.J., 2010. Gut inflammation provides a respiratory electron acceptor for Salmonella. Nature 467 (7314), 426–429.
Winter, S.E., Winter, M.G., Xavier, M.N., Thiennimitr, P., Poon, V., Keestra, A.M., Laughlin, R.C., Gomez, G., Wu, J., Lawhon, S.D., Popova, I.E., Parikh, S.J., Adams, L. G., Tsolis, R.M., Stewart, V.J., Baumler, A.J., 2013. Host-derived nitrate boosts growth of E. coli in the inflamed gut. Science 339 (6120), 708–711.
Xie, M., Fussenegger, M., 2018. Designing cell function: assembly of synthetic gene circuits for cell biology applications. Nat. Rev. Mol. Cell Biol. 19 (8), 507–525.
Yeom, S.-J., Kim, M., Kwon, K.K., Fu, Y., Rha, E., Park, S.-H., Lee, H., Kim, H., Lee, D.-H., Kim, D.-M., Lee, S.-G., 2018. A synthetic microbial biosensor for high-throughput screening of lactam biocatalysts. Nat. Commun. 9 (1), 5053.
Zhu, W., Winter, M.G., Byndloss, M.X., Spiga, L., Duerkop, B.A., Hughes, E.R., Buttner, L., de Lima Romao, E., Behrendt, C.L., Lopez, C.A., Sifuentes-Dominguez, L., Huff-Hardy, K., Wilson, R.P., Gillis, C.C., Tukel, C., Koh, A.Y., Burstein, E., Hooper, L.V., Baumler, A.J., Winter, S.E., 2018. Precision editing of the gut microbiota ameliorates colitis. Nature 553 (7687), 208–211.